

Chiral magnetic effect without chirality source in asymmetric Weyl semimetals

Dmitri E. Kharzeev^{1,2,3,*}, Yuta Kikuchi^{1,4,†} and René Meyer^{1,5‡}

¹ *Department of Physics and Astronomy, Stony Brook University, Stony Brook, New York 11794-3800, USA*

² *Department of Physics, Brookhaven National Laboratory, Upton, New York 11973-5000*

³ *RIKEN-BNL Research Center, Brookhaven National Laboratory, Upton, New York 11973-5000*

⁴ *Department of Physics, Kyoto University, Kyoto 606-8502, Japan and*

⁵ *Institute of Theoretical Physics and Astrophysics,
University of Würzburg, 97074 Würzburg, Germany*

(Dated: February 5, 2019)

We describe a new type of the Chiral Magnetic Effect (CME) that should occur in Weyl semimetals with an asymmetry in the dispersion relations of the left- and right-handed chiral Weyl fermions. In such materials, time-dependent pumping of electrons from a non-chiral external source generates a non-vanishing chiral chemical potential. This is due to the different capacities of the left- and right-handed (LH and RH) chiral Weyl cones arising from the difference in the density of states in the LH and RH cones. The chiral chemical potential then generates, via the chiral anomaly, a current along the direction of an applied magnetic field even in the absence of an external electric field. The source of chirality imbalance in this new setup is thus due to the band structure of the system and the presence of (non-chiral) electron source, and not due to the parallel electric and magnetic fields. We illustrate the effect by an argument based on the effective field theory, and by the chiral kinetic theory calculation for a rotationally invariant Weyl semimetal with different Fermi velocities in the left and right chiral Weyl cones; we also consider the case of a Weyl semimetal with Weyl nodes at different energies. We argue that this effect is generically present in Weyl semimetals with different dispersion relations for LH and RH chiral Weyl cones, such as SrSi₂ recently predicted as a Weyl semimetal with broken inversion and mirror symmetries, as long as the chiral relaxation time is much longer than the transport scattering time.

I. INTRODUCTION

The chiral magnetic effect (CME) [1] (see [2, 3] for reviews and additional references) is a non-dissipative quantum transport phenomenon induced by the chiral anomaly in the presence of an external magnetic field. It has been predicted to occur in Dirac and Weyl semimetals (DSMs/WSMs) [1, 4–9], and has been recently experimentally observed through the measurement of negative longitudinal magnetoresistance in DSMs [10–13] as well as WSMs [14–19]. In these materials, the electric current flows along the external magnetic field \mathbf{B} in the presence of a chiral chemical potential μ_5 ,

$$\mathbf{j}_{\text{CME}} = \frac{e^2}{2\pi^2} \mu_5 \mathbf{B}. \quad (1)$$

The chiral chemical potential can be formally introduced through the axion field linearly dependent on time, $\theta(t, \mathbf{x}) = -2\mu_5 t$; Eq. (1) then emerges [20] as a direct consequence of the chiral anomaly from the Chern-Simons effective action that will be considered in Section II. The CME (1) relies on a source of chirality to generate the chiral chemical potential μ_5 . In the conventional realization of CME in DSMs and WSMs, the external electric and magnetic field provide such a source via the chiral

anomaly, [21]

$$\frac{d\rho_5}{dt} = \frac{e^2}{4\pi^2 \hbar^2 c} \mathbf{E} \cdot \mathbf{B} - \frac{\rho_5}{\tau_5}, \quad (2)$$

where τ_5 is a time scale describing chiral relaxation processes present due to spin impurities, edge modes (Fermi arcs) and band mixing (described in the effective field theory by higher-dimension ultraviolet (UV) operators). With the chiral relaxation term, (2) allows for a time independent solution with finite ρ_5 if and only if the electric field has a component parallel to the magnetic field. The induced chiral chemical potential then gives rise, via (1), to the observed longitudinal magnetoconductivity growing as a square of magnetic field.

Recently, a new class of Weyl semimetals with broken reflection and inversion symmetries was predicted, with SrSi₂ as an example [22]. For brevity, we will refer to these materials as *asymmetric WSMs* (aWSMs). The authors of [22] pointed out that aWSMs, in which the Weyl points with different chiral charges have different dispersion relations, are well suited for the studies of CME.

In this paper we point out that the aWSMs indeed enable a new type of the CME that does not require an electric field, but instead is driven by an external source of electrons (we will call it *asymmetric CME*, aCME). The induced aCME current is a direct signature of the chiral anomaly responsible for Eq. (1).

The chirality source is built into the band structure of the aWSM by means of asymmetric, i.e. non-identical, dispersion relations of the left and right chiral Weyl

* dmitri.kharzeev@stonybrook.edu

† yuta.kikuchi@stonybrook.edu

‡ rene.meyer@physik.uni-wuerzburg.de

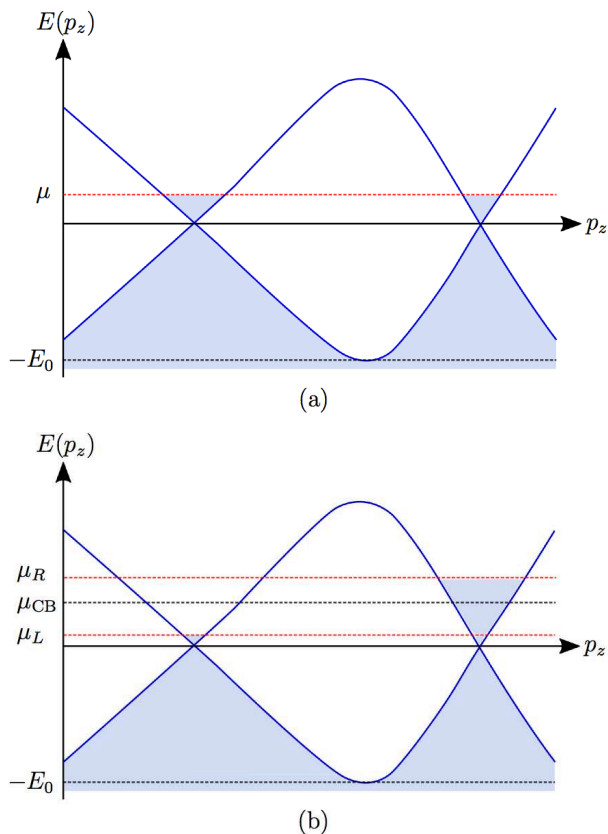


FIG. 1. (Color online) Schematic band structures of the asymmetric WSM possessing a pair of Weyl cones with different Fermi velocities for left and right. Fermi-sea contribution is regularized by a cutoff $-E_0$ determined by a bottom of the lower band. (a) Chirally balanced, i.e., equilibrium state with Fermi energy E_F . (b) Chirally imbalanced, i.e., non equilibrium state with different Fermi energies $E_{F,L}$ and $E_{F,R}$ for left and right Weyl nodes.

cones, see Fig. 1 for illustration of the special case of rotationally invariant Weyl cones with different Fermi velocities. The asymmetry in the dispersion relations leads to a different density of states (per unit chemical potential) in the left and right Weyl cones, and hence to a different capacity for quasi-particles of different chiralities.

The chirality imbalance can then be generated by pumping the system with a non-chiral time-dependent AC current, changing the chemical potential in the left and right chiral Weyl cones at a different rate due to their different capacities, which in turn induces a chiral chemical potential leading to the aCME current (1).

As an analogue of this effect, imagine two water buckets with different base areas. Obviously, the thinner bucket with smaller base area will fill up at a faster rate compared to the thicker one, if the same water inflow is applied to both. The difference in the water levels in “left” and “right” buckets in this analogy corresponds to the chiral chemical potential. As for the conventional

CME, chiral relaxation processes reduce the build up in chiral charge density (or in water level difference in our analogy), allowing for a quasi stationary non equilibrium state if the pumping rate is small compared to the chiral relaxation rate, i.e. if the pumping is adiabatic.

Weyl and Dirac semimetals can be classified in terms of the discrete symmetries of the Lorentz group [23–26]: parity (P), that coincides with inversion (I) in odd number of spatial dimensions, and time reversal (T). Separating left and right chiral Weyl nodes along a vector \mathbf{b} in momentum space breaks T but preserves P, while separating the nodes in energy only (but not in momentum) by an amount b_0 preserves T and breaks P. A WSM hence necessarily breaks either P or T, or both, as in Fig. 2. A DSM, on the other hand, preserves both P and T. Left- and right-handed Weyl fermions are bound to exist in pairs in a lattice system due to the Nielsen-Ninomiya theorem [27–29] or, in other words, since the Berry curvature of the Brillouin zone as a whole has to vanish [30].

The above classification in terms of P and T assumes identical dispersion relations for the left- and right-handed chiral particles. Parity exchanges left and right chiralities, and hence is broken explicitly if the dispersion relations of the left and right chiral Weyl fermions are not identical [31]. Thus, every perturbation of the band structure leading to the difference between the low energy dispersion relations of left- and right-handed particles will break parity.

Asymmetric Weyl semimetals (aWSMs) possess such a parity non-invariant pair of Weyl cones with opposite chiralities. A specific realization of aWSM has been proposed recently in [22]. aWSMs constitute a new distinct class of WSMs, and topological semimetals in general. Since in condensed matter systems Lorentz invariance and in particular rotational invariance is not a fundamental but rather an emergent symmetry at low energies, aWSMs can be expected to occur quite generically.

An interesting (and well controlled theoretically) way of breaking parity and Lorentz symmetry [32] while preserving rotational invariance is to introduce different Fermi velocities for the left and right Weyl cones, as depicted schematically in Fig. 1. In high energy physics, this would correspond to a (rather pathological) universe in which left- and right-handed massless chiral electrons move at a different speed, so there is no unique speed of light.

In the main part of this paper we will focus on this particular example of an asymmetric WSM for the derivation of the novel chiral magnetic effect. However, to the best of our knowledge, candidate WSMs with different Fermi velocities for otherwise approximately undeformed left and right chiral Weyl cones have yet to be discovered. On the other hand, WSMs with approximately rotationally invariant Weyl nodes and approximately equal Fermi velocities which are separated not only in momentum but also in energy (c.f. Fig. 2) do exist [22] and, as we will show in App. C, also admit the same asymmetric CME due to the different number of states filled below

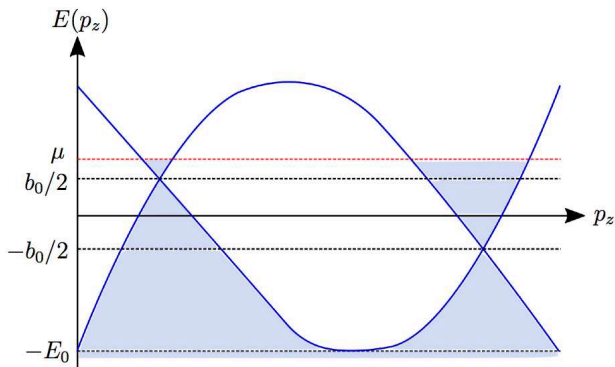


FIG. 2. (Color online) Schematic band structures of the asymmetric WSM, which possesses a pair of Weyl cones with finite energy difference b_0

the Fermi level. Finally, we will argue in Sec. VI that the qualitative effect should exist generically for asymmetric WSMs in which the capacity of the left and right chiral Weyl nodes is different, and chiral relaxation is slow compared to other transport time scales.

From the point of view of chiral kinetic theory it is clear that an asymmetric deformation of the Weyl cones does not affect anomalous transport phenomena such as the CME (1) since the singular structure of the band touchings in momentum space, the Berry monopole, is invariant under such small deformations. We will indeed confirm in Sec. III and App. C that in the cases considered here the chiral kinetic expression for the CME current remains of the form (1). It seems however nontrivial in terms of field theory, where the anomaly is caused by subtle ultraviolet (UV) properties, and the absence of Lorentz invariance in the UV a priori may lead to a modification of the anomaly. For this reason, we calculate in Sec. II the effective action in the case of different Fermi velocities for left and right chiral Weyl nodes, and show that (1) is unchanged also in this approach. Although this does not constitute a proof for the general case, it gives us confidence that, as expected from the anomaly matching arguments [33, 34], the chiral magnetic current should always be of form (1) as long as Lorentz symmetry is restored for each Weyl node separately at low energies.

In order to induce a finite current response from (1), a chiral chemical potential μ_5 needs to be induced. In the conventional CME this is achieved by an external electric field with a component parallel to the external magnetic field which, as discussed above, via the chiral anomaly induces a chiral charge density (2) and hence a chiral chemical potential. In the new asymmetric CME in asymmetric WSMs proposed here, the chiral chemical potential is generated by a completely different mechanism, briefly described above and discussed in detail in Sec. IV for the case of asymmetric Fermi velocities: The chiral charge imbalance is realized by injecting chirally neutral and electrically charged particles (such as the electrons

coming from the household electric outlet) into the asymmetric WSM at a given rate, i.e. by changing the charge density $\rho(t)$ in a time-dependent way.

As discussed in Sec. V (c.f. Fig. 3), this can be achieved experimentally for example by applying an AC voltage to the grounded sample, inducing a time-dependent change in the chemical potential $\mu(t)$. At first one may think that this does not induce a chiral chemical potential, and hence no chiral charge density. However, the different capacities of the left and right handed Weyl nodes of an asymmetric WSM, described by the different equations of state $\rho_{L/R}(\mu_{L/R}, T, \dots)$ [35], do allow for a non vanishing chiral charge density $\rho_5 = \rho_L - \rho_R$ even for vanishing chiral chemical potential $\mu_5 = (\mu_L - \mu_R)/2 = 0$. The contributions from $\rho_{L/R}$ to ρ_5 in this case do not exactly cancel each other due to the spectral asymmetry between the left and right Weyl nodes, as e.g. for unequal Fermi velocities depicted in Fig. 1,

$$\rho_{L/R} = \frac{\mu_{L/R}^3 + E_0^3}{6\pi^2 v_{L/R}^3}. \quad (3)$$

This is also true in equilibrium (i.e in a time independent configuration with $\mu_5 = 0$), in which an asymmetric WSM has a non-vanishing chiral charge density $\rho_5 \equiv \rho_L - \rho_R$ that does not vanish even at $\mu_5 = 0$, c.f. (3) for the case of $v_L \neq v_R$. In equilibrium and in the absence of the chiral anomaly, however, this chiral charge density is conserved and does not lead to any electrical transport.

If, on the other hand, the chemical potential $\mu(t)$ is changed in a time-dependent way by pumping non chiral electrons into or out of the system, a time dependent charge density $\rho(t)$ will be induced, as well as the chiral charge density $\rho_5(t)$. However if the chiral relaxation rate is larger than the charge pumping rate, the resulting state will be characterized by the vanishing chiral chemical potential, see Fig. 1(a). We will call this state *chirally balanced* even though it possesses non-zero chiral charge density ρ_5 . The chiral charge density in this state is defined as $\rho_5^{\text{CB}}(t) \equiv \rho_5(\mu_5 = 0, \dots)$, where CB stands for “chirally balanced”, and the dots represent other parametric dependencies. However, the so-induced $\rho(t)$ and $\rho_5^{\text{CB}}(t)$ are now time dependent and hence not trivially conserved any longer. This is expected for the charge density $\rho(t)$, as it is pumped externally by the nonchiral current. In the absence of the anomaly, however, there is no obvious source of nonconservation for the chiral charge density $\rho_5^{\text{CB}}(t)$. In order to saturate the conservation law for the chiral charge density, there hence needs to exist another component of the chiral charge density, which we call $\delta\rho_5(t)$ (c.f. eq. (30) and (31)). The chiral chemical potential $\mu_5(t)$ induced by $\delta\rho_5(t)$ then generates the aCME current response via (1). This response is directly proportional to the rate of change of the chemical potential $\frac{d\mu}{dt}$ times the chiral relaxation time τ_5 , as expected for a quasi stationary nonequilibrium state driven by the change in chemical potential and stabilized by the chiral relaxation rate.

This paper is organized as follows. In Sec. II, the effective action describing anomalous electric transport phenomena such as the CME are derived in the case of an asymmetric WSM induced by different Fermi velocities for the left and right chiral Weyl nodes. In Sec. III, we derive the aCME current at zero temperature from chiral kinetic theory and show that it reproduces the result of the field theoretic derivation of Sec. II. Sections IV and V are the main part of this paper. In Sec. IV, we derive from the equation of state (3) for unequal Fermi velocities the relation between applied pumping rate and induced chiral chemical potential which in turn induces the aCME current. In Sec. V, we discuss an experimental setup needed to observe the aCME in asymmetric WSMs and give a quantitative estimate of the current density. Sec. VI is devoted to a summary and conclusions. In particular we discuss a class of asymmetric WSMs (we call them chirally imbalanced materials) that should exhibit the aCME.

Technical details are relegated to several Appendices. In App. A, we present the detailed calculation of the index necessary to arrive at the effective action of Sec. II. In App. B, we extend our chiral kinetic theory calculations of the asymmetric CME current discussed in Sec. III and IV to finite temperatures. We find that for the case of asymmetric Fermi velocities the finite temperature contributions cancel in the final result, and comment on the non generality of such cancellations. In App. C we derive and estimate the asymmetric CME in WSMs with Weyl nodes separated not only in momentum but also in energy, as depicted in Fig. 2. The conversion from natural into Gaussian units and the estimate of the asymmetric CME currents are summarized in App. D.

II. CHERN-SIMONS EFFECTIVE ACTION AND TOPOLOGICAL RESPONSE

WSMs are topological materials possessing chiral Weyl nodes separated in momentum and/or energy; the anomalous response of these materials to external field is described by the Chern-Simons action. As already discussed in Sec. I, the CME (1) is induced by the chiral chemical potential μ_5 . As will be reiterated below, the chiral anomaly indeed generates the Chern-Simons term which leads to the CME current (1). Conventional WSMs (i.e. the ones possessing identical dispersion relations for left- and right-handed fermions) are described by the following action for a four component Dirac spinor ψ in Euclidean signature

$$\begin{aligned} S &= \int d\tau d\mathbf{r} \bar{\psi} i(\not{D} + i\not{b}\gamma_5) \psi \\ &= \int d\tau d\mathbf{r} \bar{\psi} \begin{pmatrix} 0 & i\bar{\sigma}^\mu(D_\mu - ib_\mu) - \mu_5 \\ i\sigma^\mu(D_\mu + ib_\mu) + \mu_5 & 0 \end{pmatrix} \psi, \end{aligned} \quad (4)$$

where $\not{D} \equiv \gamma^\mu D_\mu$ and $\not{b} \equiv \gamma^\mu b_\mu$. γ^μ ($\mu = 0, 1, 2, 3$) denotes Dirac matrices, and $\sigma^\mu = (1, \sigma^i)$ and $\bar{\sigma}^\mu = (1, -\sigma^i)$ are defined via the Pauli matrices σ^i ($i = 1, 2, 3$). Here, b^μ represents the separation between the two Weyl nodes in energy-momentum space. It should be emphasized [7] that μ_5 , which is induced by non equilibrium processes, contributes to the CME response (1), while b_0 is a part of parameterizations of the band structure and hence does not directly lead to persistent current via (1) [36]. By performing the chiral gauge transformations

$$\psi_{L/R} \rightarrow e^{-i\theta(x)\gamma_5/2} \psi_{L/R} = e^{-i\theta(x)(\gamma_5 \pm 1)/4} \psi_{L/R}, \quad (5)$$

$$\bar{\psi}_{L/R} \rightarrow \bar{\psi}_{L/R} e^{-i\theta(x)\gamma_5/2} = \bar{\psi}_{L/R} e^{-i\theta(x)(\gamma_5 \mp 1)/4}, \quad (6)$$

with $\theta = -2\mu_5 t$ in the action (4), μ_5 terms are rotated away and the Chern-Simons action

$$S_{CS} = \frac{e^2}{32\pi^2} \int d^4x \theta(x) \epsilon^{\mu\nu\alpha\beta} F_{\mu\nu} F_{\alpha\beta} \quad (7)$$

is generated.

Following the discussion given in [6, 37], we now consider an effective action for the asymmetric WSM where the Fermi velocities of left and right chiral fermions respectively, v_L and v_R , take different values (c.f. Fig. 1). In this case, the action (4) is modified as

$$S = \int d\tau d\mathbf{r} \bar{\psi} \begin{pmatrix} 0 & i\tilde{D}_R + \mu_5 \\ i\tilde{D}_L - \mu_5 & 0 \end{pmatrix} \psi. \quad (8)$$

Here, we have defined covariant derivatives

$$\begin{aligned} \tilde{D}_L &= (D_0 + ib_0) - v_L \sigma^i (D_i + ib_i), \\ \tilde{D}_R &= (D_0 - ib_0) + v_R \bar{\sigma}^i (D_i - ib_i), \end{aligned} \quad (9)$$

which are 2×2 component matrices. Eq. (8) can be rewritten with use of four-component Weyl spinors ψ_L and ψ_R satisfying $\gamma_5 \psi_{L/R} = \pm \psi_{L/R}$,

$$\begin{aligned} S &= \int d\tau d\mathbf{r} [\bar{\psi}_L i(\not{D}_L - i\mu_5 \gamma^0 \gamma_5) \psi_L \\ &\quad + \bar{\psi}_R i(\not{D}_R - i\mu_5 \gamma^0 \gamma_5) \psi_R], \end{aligned} \quad (10)$$

where covariant derivatives are now defined as [38]

$$\not{D}_{L/R} = [\gamma^0 (D_0 + ib_0 \gamma_5) + v_{L/R} \gamma^i (D_i + ib_i \gamma_5)]. \quad (11)$$

We will now show that the chiral gauge transformation (5) and (6) yields the conventional four dimensional Chern-Simons term (7) despite the asymmetric deformation of the Dirac action. In particular, the chiral chemical potential term in (10) can be rotated away by a chiral rotation with $\theta = -2\mu_5 t$, in which case (10) describes the magnetic response of the aWSM to non vanishing μ_5 .

Let us first focus on the left-handed fermion part of the action (10). ψ_L and $\bar{\psi}_L$ can be decomposed in terms of Dirac eigenfunctions $\{\phi_n\}$, such that $\not{D}_L \phi_n = \lambda_n \phi_n$, as

$$\psi_L = \sum_n \phi_n c_n, \quad \bar{\psi}_L = \sum_n \phi_n^* \bar{c}_n. \quad (12)$$

Infinitesimal chiral rotations of c and \bar{c} are specified from Eqs. (5) and (6),

$$c'_n = \sum_m U_{nm} c_m, \\ U_{nm} = \delta_{nm} - \frac{i}{4} \int d^4x \phi_n^*(x) \theta(x) (\gamma_5 \pm 1) \phi_m(x), \quad (13)$$

$$\bar{c}'_n = \sum_m V_{mn} \bar{c}_m, \\ V_{mn} = \delta_{mn} - \frac{i}{4} \int d^4x \phi_m^*(x) \theta(x) (\gamma_5 \mp 1) \phi_n(x). \quad (14)$$

Henceforth, the Jacobian of the chiral gauge transformation becomes

$$\det(U^{-1}V^{-1}) = \exp\left(\frac{i}{2} \int d^4x \theta(x) \sum_n \phi_n^*(x) \gamma_5 \phi_n(x)\right). \quad (15)$$

The right hand side of the above equation includes the expression of the index for a single left chiral fermion,

$$\sum_n \phi_n^*(x) \gamma_5 \phi_n(x) = \frac{e^2}{32\pi^2} \epsilon^{\mu\nu\alpha\beta} F_{\mu\nu} F_{\alpha\beta}. \quad (16)$$

where $\epsilon^{\mu\nu\alpha\beta}$ is the antisymmetric tensor and the field strength is defined by $F_{\mu\nu} = \partial_\mu A_\nu - \partial_\nu A_\mu$. The detailed calculation of the index is presented in App. A. Notice that (16) does not depend on the Fermi velocity v_L , which cancels out during the calculation (App. A). The chiral gauge transformation for the right chiral action gives the same expression as (15) and (16). Therefore, by combining the Jacobians caused by the left and right chiral gauge transformations we obtain the usual Chern-Simons term as an effective action (7)

$$S_{\text{CS}} = -\frac{e^2}{8\pi^2} \int d^4x \epsilon^{\mu\nu\alpha\beta} \partial_\mu \theta(x) A_\nu \partial_\alpha A_\beta, \quad (17)$$

where we have integrated by parts in (7) and neglected the surface term. By taking the derivative with respect to A_i and setting $\theta = -\mu_5 t$, we obtain the the anomaly induced current

$$j_i = \frac{\delta S_{\text{CS}}}{\delta A_i} = \frac{e^2}{2\pi^2} \mu_5 \epsilon^{0i\alpha\beta} \partial_\alpha A_\beta = \frac{e^2}{2\pi^2} \mu_5 B_i. \quad (18)$$

This expression for the chiral magnetic current agrees with that of conventional WSMs. We will see in the next section that chiral kinetic theory yields the same result.

III. CHIRAL KINETIC APPROACH

In this section, we use chiral kinetic theory to describe the CME in asymmetric WSMs with different Fermi velocities. Chiral kinetic theory allows to describe the non equilibrium states considered here by incorporating the

chiral anomaly via to geometric Berry phase (Berry curvature) [4, 39] of the Weyl nodes into kinetic theory.

In aWSMs, the excitations close to left and right chiral Weyl nodes are described by the following Hamiltonian,

$$H_{L/R} = \pm v_{L/R} \boldsymbol{\sigma} \cdot (\mathbf{p} \pm \mathbf{b}/2), \quad (19)$$

where \mathbf{b} represents the spatial separation between the left and right Weyl nodes in momentum space. In this and following sections, we consider the effect of the different Fermi velocities v_L and v_R , and the energy difference between a pair of Weyl nodes is set to zero ($b_0 = 0$) for simplicity. Although nonvanishing b_0 does not affect the result (26), it plays an important role in inducing chiral chemical potential as briefly discussed in Sec.s IV and V; a more detailed discussion is presented in App. C.

Let us concentrate on the left-handed chiral part. Diagonalizing H_L yields two eigenenergies, $\epsilon_\pm = \pm v_L |\mathbf{p} + \mathbf{b}/2|$ with corresponding eigenvectors

$$u_{\pm, \mathbf{p}} = \frac{1}{\sqrt{2|\mathbf{p} + \mathbf{b}/2|(|\mathbf{p} + \mathbf{b}| \mp (p_z + b_z/2))}} \\ \times \begin{pmatrix} (p_x + b_x/2) - i(p_y + b_y/2) \\ \pm |\mathbf{p} + \mathbf{b}/2| - (p_z + b_z/2) \end{pmatrix}, \quad (20)$$

respectively. The Berry connection \mathcal{A} and Berry curvatures Ω for these states are given by

$$\mathcal{A} \equiv -i u_{\pm, \mathbf{p}}^\dagger \nabla_{\mathbf{p}} u_{\pm, \mathbf{p}}, \quad (21)$$

$$\Omega \equiv \nabla \times \mathcal{A} = \pm \frac{\mathbf{p} + \mathbf{b}/2}{2|\mathbf{p} + \mathbf{b}/2|^3}. \quad (22)$$

Eq. (22) describes a geometric structure in momentum space. One can see that a monopole (antimonopole) is located at $\mathbf{p} = -\mathbf{b}/2$ corresponding to the positive (negative) energy part of the left Weyl cone. Similarly, the positive (negative) energy right Weyl cone gives an anti-monopole (monopole) at $\mathbf{p} = \mathbf{b}/2$. The monopole charges due to the left and right Weyl nodes sum up to zero in accord with Nielsen-Ninomiya theorem [27–29].

Notice that the chiral kinetic approach breaks down around the monopole singularities located at the nodal points of the Weyl cones where the quantum anomaly violates the semiclassical description. To avoid these singularities, the typical momentum of the quasi particles described in kinetic theory should be outside the quantum region around the nodal points. For example, in near equilibrium systems at zero temperature, the momentum of the quasi particle is characterized by the chemical potential μ , while the typical radius of quantum region is $\sqrt{|\mathbf{B}|}$. Therefore, $\sqrt{|\mathbf{B}|} \ll \mu$ should be satisfied, which implies that strong magnetic field invalidates the chiral kinetic approach.

In chiral kinetic theory, the CME current is expressed as [4, 39, 40]

$$j_{\text{CME}} = e^2 \mathbf{B} \int_{\mathbf{p}} f_{\mathbf{p}} \left(\boldsymbol{\Omega} \cdot \frac{\partial \epsilon_{\mathbf{p}}}{\partial \mathbf{p}} \right), \quad (23)$$

where $\int_{\mathbf{p}} \equiv \int d^3\mathbf{p}/(2\pi)^3$ and $f_{\mathbf{p}}(x)$ is the one body distribution function. Now, we calculate the left chiral contribution to the CME current at vanishing temperature. An extension to finite-temperature is straightforward (c.f. App. B). The equilibrium distribution function at zero temperature is given by $\Theta(\mu_L - \epsilon_{\mathbf{p}})$. Eq. (23) is then evaluated as

$$\begin{aligned} j_{\text{CME},L} &= e^2 \mathbf{B} \int_{\mathbf{p}} \Theta(\mu_L - \epsilon_{\mathbf{p}}) \left(\boldsymbol{\Omega} \cdot \frac{\partial \epsilon_{\mathbf{p}}}{\partial \mathbf{p}} \right) \\ &= \frac{e^2 \mathbf{B}}{4\pi^2} (\mu_L + E_0), \end{aligned} \quad (24)$$

where $-E_0$ is the physical cutoff determined by the band structure as depicted in Fig. 1 [7]. Similarly, the right chiral Weyl node yields

$$j_{\text{CME},R} = -\frac{e^2 \mathbf{B}}{4\pi^2} (\mu_R + E_0), \quad (25)$$

which has the opposite sign compared with the left contribution due to the opposite monopole charge. Therefore, the total CME current is given by

$$j_{\text{CME}} = \frac{e^2 \mu_5}{2\pi^2} \mathbf{B}, \quad (26)$$

with the chiral chemical potential $\mu_5 \equiv (\mu_L - \mu_R)/2$. This expression agrees with that obtained from the effective CS action (18).

IV. PUMPING-INDUCED CHIRALITY IMBALANCE IN ASYMMETRIC WSM

In this section, we describe a way to induce the chirality imbalance by pumping electrons into the asymmetric WSM. Since the pumped current is chirally neutral, the left and right chiral charge densities increase at the same rate. A detailed experimental setup will be discussed in Sec. V. We assume that due to pumping the total particle number density is time-dependent, $\rho = \rho(t)$. The particle number densities and chemical potentials for each Weyl node are related by

$$\rho_{L/R} = \int_{\mathbf{p}} \Theta(\mu_{L/R} - v_{F,L/R} |\mathbf{p}|) = \frac{\mu_{L/R}^3 + E_0^3}{6\pi^2 v_{L/R}^3}, \quad (27)$$

and the chiral charge density is given by $\rho_5 = \rho_L - \rho_R$. In a *chirally balanced* state, defined by a state satisfying $\mu_L = \mu_R \equiv \mu_{\text{CB}}(t)$, the left and right chiral particle densities are $\rho_{L/R}^{\text{CB}} = \rho_{L/R}(\mu_{L/R} = \mu_{\text{CB}})$ and the total number density $\rho = \rho_L^{\text{CB}} + \rho_R^{\text{CB}}$ is given by

$$\rho = \frac{\mu_{\text{CB}}^3 + E_0^3}{6\pi^2} \left(\frac{1}{v_L^3} + \frac{1}{v_R^3} \right) = \rho(t), \quad (28)$$

which leads to the following expression for the chiral density in the chirally balanced state,

$$\rho_5^{\text{CB}} = -\rho(t) \frac{v_L^3 - v_R^3}{v_L^3 + v_R^3} + \text{const.} \quad (29)$$

Here we neglect a time independent constant involving the Dirac sea cutoff E_0 . It is noteworthy that $\mu_5 = \mu_L - \mu_R = 0$ in the chirally balanced state, although ρ_5^{CB} is finite due to the different capacities between two Weyl cones. Since the pumping current is not chiral, the chiral charge density is conserved,

$$\frac{d\rho_5}{dt} = 0. \quad (30)$$

The anomalous contribution is absent because $\mathbf{E} \cdot \mathbf{B} = 0$. The chiral density ρ_5 can be decomposed as $\rho_5 = \rho_5^{\text{CB}} + \delta\rho_5$, respectively. With the use of (29), (30) can then be rewritten as

$$\frac{d\delta\rho_5}{dt} = \frac{d\rho(t)}{dt} \frac{v_L^3 - v_R^3}{v_L^3 + v_R^3} - \frac{\delta\rho_5}{\tau_5}, \quad (31)$$

where we have added the last term on the right hand side to describe the chirality relaxation towards the chirally balanced state with chiral density ρ_5^{CB} .

Competition between the generation of chirality imbalance induced by the particle pumping and the chiral relaxation results in a late time solution of (31) at $t \gg \tau_5$. Aiming at describing an experimental measurement, we assume oscillatory particle pumping, i.e., $\rho(t) = \bar{\rho} + \delta\rho(t)$ with $\delta\rho(t) \propto e^{i\omega t}$. Then, the late time solution of (31) is

$$\delta\rho_5 = \frac{\tau_5}{1 + i\omega\tau_5} \frac{d\rho(t)}{dt} \frac{v_L^3 - v_R^3}{v_L^3 + v_R^3}, \quad (32)$$

We now relate this solution to the chiral chemical potential. To this end, we consider the quantity $v_L^3 \delta\rho_L - v_R^3 \delta\rho_R$, which can be converted in two different ways,

$$\begin{aligned} v_L^3 \delta\rho_L - v_R^3 \delta\rho_R &= \frac{v_L^3 - v_R^3}{2} \delta\rho + \frac{v_L^3 + v_R^3}{2} \delta\rho_5 \\ &= \frac{\tau_5}{1 + i\omega\tau_5} \frac{d\rho(t)}{dt} \frac{v_L^3 - v_R^3}{2}, \end{aligned} \quad (33)$$

$$\begin{aligned} v_L^3 \delta\rho_L - v_R^3 \delta\rho_R &= \frac{\mu_L^3 - \mu_R^3}{6\pi^2} = \frac{3\mu^2 \mu_5 - \mu_5^3}{3\pi^2} \\ &\simeq \frac{\mu^2 \mu_5}{\pi^2} (1 + O((\mu_5/\mu)^2)). \end{aligned} \quad (34)$$

where $\mu = (\mu_L + \mu_R)/2$ and $\mu_5 = (\mu_L - \mu_R)/2$, and we have assumed that $\mu_5 \ll \mu$. Combining these two equations yields the expression for the chiral chemical potential,

$$\mu_5 \simeq \frac{\pi^2 (v_L^3 - v_R^3)}{2\mu^2} \frac{\tau_5}{1 + i\omega\tau_5} \frac{d\rho(t)}{dt}. \quad (35)$$

In addition, the relation between the particle number density and chemical potential becomes

$$\begin{aligned} \rho(t) &= \frac{1}{6\pi^2} \left(\frac{\mu_L^3 + E_0^3}{v_L^3} + \frac{\mu_R^3 + E_0^3}{v_R^3} \right) \\ &= \frac{\mu^3 + E_0^3}{6\pi^2} \left(\frac{1}{v_L^3} + \frac{1}{v_R^3} \right) \left(1 + O\left(\frac{\Delta v}{V} \frac{\mu_5}{\mu} \right) \right). \end{aligned} \quad (36)$$

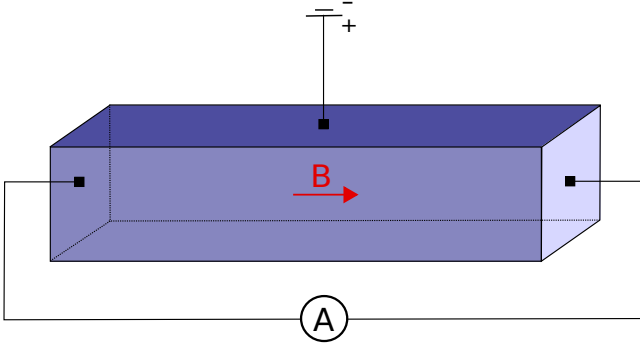


FIG. 3. (Color online) Experimental setup to measure the aCME current. The material is put into a homogeneous external magnetic field. The chemical potential is changed by applying a time dependent voltage to the gate, which pumps the system with non chiral electrons. The current is then measured through two gates applied in the direction of the external field. Alternatively, the voltage drop through the sample could be measured instead.

where we have defined $\Delta v \equiv v_L - v_R$ and $V \equiv (v_L + v_R)/2$ and picked up the leading order of $\Delta v/V$ in the final expression. Therefore, the chiral chemical potential is given by

$$\mu_5 = \frac{(v_L^6 - v_R^6)}{4v_L^3 v_R^3} \frac{\tau_5}{1 + i\omega\tau_5} \frac{d\mu}{dt} \simeq \frac{3}{2} \frac{\Delta v}{V} \frac{\tau_5}{1 + i\omega\tau_5} \frac{d\mu}{dt}. \quad (37)$$

Let us reiterate that the chiral chemical potential is induced by the different Fermi velocities for left and right Weyl nodes in this mechanism, due to the different capacity of electron states in the two Weyl cones. The mechanism is distinct from the conventional one in the symmetric WSM, where the chiral chemical potential is generated by an external electric field component parallel to the external magnetic field, i.e. by $\mathbf{E} \cdot \mathbf{B}$.

Finally, inserting (37) into (26), we obtain the expression for the aCME current,

$$\mathbf{j}_{\text{CME}} = \frac{3e^2}{4\pi^2} \frac{\Delta v}{V} \frac{\tau_5}{1 + i\omega\tau_5} \frac{d\mu}{dt} \mathbf{B}. \quad (38)$$

As shown in App. B, this expression does not receive finite-temperature corrections up to $O((\mu_5/\mu)(\Delta v/V))$ due to cancellations present for the case of different Fermi velocities. These cancellations are however tied to the particular choice of dispersion relation, as evident from the aCME current (C8) for a chiral pair of Weyl nodes separated in energy by a amount b_0 (c.f. Fig. 2) derived in App. C, where no such cancellations happen.

V. EXPERIMENTAL SETUP

The predictions for the aCME currents (38) and (C8) can be experimentally verified by the simple experimental setup depicted in Fig. 3. The sample, ideally a slab of a

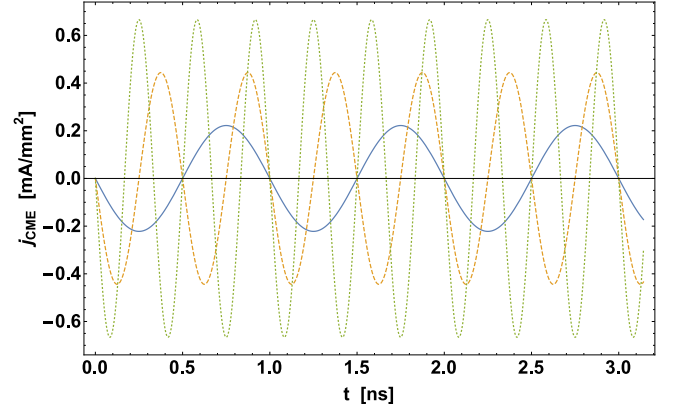


FIG. 4. (Color online) Current density response (B10) for $\Delta = 50$ meV, $\Delta v/V = 0.1$, $|\mathbf{B}| = 1$ T, and $|\delta\mu| = 1$ meV, and frequencies $\omega = 1$ GHz (blue solid), 2 GHz (yellow dashed) and 3 GHz (green dotted).

single crystal, is connected to a gate providing a reservoir of electrons, and put into a constant external magnetic field. We then expect that once the AC voltage is applied to the gate, the aCME current will be generated parallel to the magnetic field. Note that such a current is absent in conventional electromagnetism.

The chemical potential entering (38) and (C8) in this setup is provided through an AC voltage that pumps electrons into the system at a rate $d\rho/dt$. The chiral relaxation time τ_5 is intrinsic to the system, and has been estimated from the conventional CME in e.g. ZrTe₅ [10] to be parametrically larger than the Ohmic current relaxation rate extracted from the Drude model, $\tau_5 \sim 10 \dots 100 \times \tau$ [41]. The advantage of this setup is that it does not measure the conventional CME, present only if \mathbf{E} has a component parallel to \mathbf{B} , but is only sensitive to the new chiral magnetic current (38).

With the result for the aCME current (38) at hand, we can now estimate the current response for aWSMs with approximate rotational invariance but different Fermi velocities on the left and right chiral Weyl cones. Reinstating \hbar and c , (38) becomes

$$\begin{aligned} \mathbf{j}_{\text{CME}} &= \frac{3e^2}{4\pi^2 \hbar^2 c} \frac{\tau_5}{1 + i\omega\tau_5} \frac{\Delta v}{V} \frac{d\mu(t)}{dt} \mathbf{B} \\ &\simeq \frac{3e^2}{4\pi^2 \hbar^2 c} \tau_5 \frac{\Delta v}{V} \frac{d\mu(t)}{dt} \mathbf{B}. \end{aligned} \quad (39)$$

Here we have employed the approximation $\omega\tau_5 \ll 1$, which is the typical regime in the experimental setup we propose here. Since the typical chiral relaxation rates are in the Terahertz regime, $\tau_5^{-1} \sim \frac{O(10\text{meV})}{\hbar} \sim \text{THz}$ [10], but the technically reachable driving frequencies are $O(\text{GHz})$ [42], $\omega\tau_5 \sim 10^{-3} \ll 1$ is well satisfied.

We now consider AC voltages that induce a time-dependent chemical potential given by $\mu(t) = \bar{\mu} + \delta\mu(t)$ with $\delta\mu \ll \bar{\mu}$. This restriction of course limits the amplitude of the driving voltages and hence the aCME current

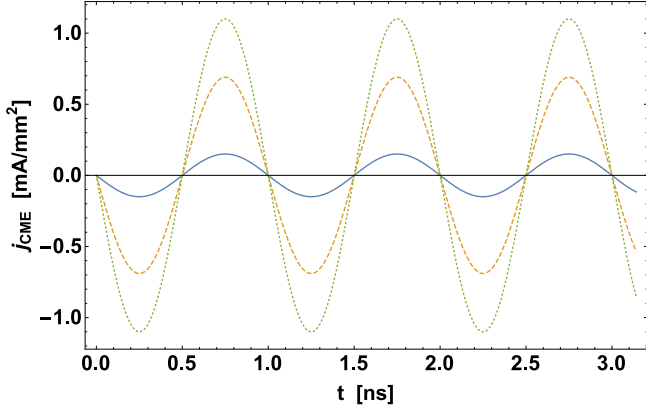


FIG. 5. (Color online) Current density response (C8) for $\Delta = 50$ meV, $\nu = 1$ GHz, $|\mathbf{B}| = 1$ T, $T = 20$ K, $\bar{\mu} = 10$ meV, and $|\delta\mu| = 1$ meV, and each curve corresponds to $b_0 = 1$ meV (blue solid), 5 meV (yellow dashed) and 10 meV (green dotted).

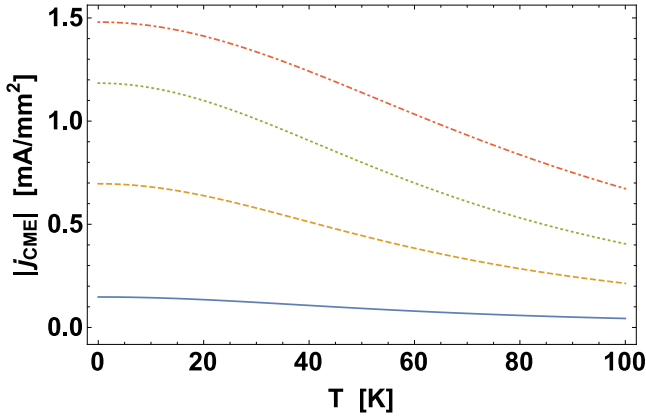


FIG. 6. (Color online) Temperature dependence of the amplitudes of current density response (C8) for $\Delta = 50$ meV, $\nu = 1$ GHz, $|\mathbf{B}| = 1$ T, $\bar{\mu} = 10$ meV, and $|\delta\mu| = 1$ meV, and each curve corresponds to $b_0 = 1$ meV (blue solid), 5 meV (yellow dashed), 10 meV (green dotted) and 20 meV (red dot-dashed).

output, but not severely: typical values for the chemical potential (see e.g. the value for ZrTe_5 derived in [10]) are expected to be $O(10 \text{ meV})$, which would allow driving voltages of $0.1 \dots 1 \text{ meV}$. We can then use (36) to find an approximate linear relationship between the time-dependent part of the chemical potential and charge density,

$$\bar{\rho} + \delta\rho(t) \simeq \frac{\bar{\mu}^3 + E_0^3}{6\pi^2} \left(\frac{1}{v_L^3} + \frac{1}{v_R^3} \right) + \frac{\bar{\mu}^2}{2\pi^2} \left(\frac{1}{v_L^3} + \frac{1}{v_R^3} \right) \delta\mu(t). \quad (40)$$

Assuming a harmonically varying chemical potential $\delta\mu(t) \propto \delta\rho(t) \propto e^{i\omega t}$, using $\omega\tau_5 \ll 1$ and taking the

real part of (38), we arrive at (c.f. App. B and App. D for the derivations of (41) and (42))

$$\mathbf{j}_{\text{CME}} = -\frac{3e^2}{4\pi^2\hbar^2c} \frac{\Delta v}{V} (\omega\tau_5) \sin(\omega t) |\delta\mu| \mathbf{B}, \quad (41)$$

$$\frac{\mathbf{j}_{\text{CME}}}{[\text{mA/mm}^2]} = -(1.1 \times 10^2) \frac{\Delta v}{V} \frac{2\pi\nu}{[\text{GHz}]} \frac{|\delta\mu|}{[\text{meV}]} \left(\frac{\Delta}{[\text{meV}]} \right)^{-1} \times \frac{\mathbf{B}}{[\text{T}]} \times \sin \left(\frac{2\pi\nu}{[\text{GHz}]} \frac{t}{[\text{ns}]} \right). \quad (42)$$

In the last line, we have converted the chiral relaxation time into an energy scale Δ via $\tau_5 = \hbar/\Delta$ and worked with frequency ν instead of angular frequency $\omega = 2\pi\nu$.

We can now estimate the magnitude of the asymmetric CME current from (42). Using as input parameters $|\delta\mu| = 1 \text{ meV}$, $\nu = 1 \text{ GHz}$, $\Delta = 50 \text{ meV}$, $\Delta v/V = 0.1$, and $B = 1 \text{ T}$, we find a current density of $|j_{\text{aCME}}| \simeq 20 \text{ mA/cm}^2$. Note that the parameters in (39) have to be given in the Gaussian (CGS) units, which are summarized in App. D. In App. D we also estimate the ordinary CME current with the same input parameters and realistic electric field strengths of 0.1 mV/mm at which the experiments in [10] were performed. The resulting CME current density $|j_{\text{CME}}| = 40 \text{ mA/cm}^2$ is comparable to the current density of our new aCME, which hence should be measurable in laboratory experiments.

The expected current density response for these input parameters is plotted in Fig. 4 for frequencies $\nu = 1 \text{ GHz}, 2 \text{ GHz}, 3 \text{ GHz}$, respectively, corresponding to the highest technically attainable frequencies. Since for typical chiral relaxation times $\tau_5 \sim \hbar/(1 \dots 10 \text{ meV}) \sim 1 \dots 10 \text{ THz}$ this is clearly in the regime $2\pi\nu\tau_5 \ll 1$, we find little additional dependence of the aCME signal on $2\pi\nu\tau_5$ besides the scaling of the amplitude of the signal with $2\pi\nu\tau_5$ as predicted by (42): In the regime $2\pi\nu\tau_5 \ll 1$, the novel CME response is predicted to be a sinusoidal signal with the same frequency as the input modulation of the gate voltage, phase shifted by $-\pi$.

In App. D we also estimated the aCME signal for the aWSM with left and right Weyl cones separated in energy by an amount b_0 (c.f. Fig. 2 and Eq. (C8)). The resulting signal

$$\frac{\mathbf{j}_{\text{CME}}}{[\text{mA/mm}^2]} = -(7.4 \times 10) \times \left(\frac{\bar{\mu}}{b_0} + 0.024 \times \left(\frac{T}{[\text{K}]} \right)^2 \left(\frac{b_0 \bar{\mu}}{[\text{meV}^2]} \right)^{-1} + \frac{b_0}{4\bar{\mu}} \right)^{-1} \times \frac{\omega}{[\text{GHz}]} \frac{|\delta\mu|}{[\text{meV}]} \left(\frac{\Delta}{[\text{meV}]} \right)^{-1} \frac{\mathbf{B}}{[\text{T}]} \sin \left(\frac{\omega}{[\text{GHz}]} \frac{t}{[\text{ns}]} \right) \quad (43)$$

is plotted in Fig. 5 for comparable input parameters $\Delta = 50 \text{ meV}$, $\nu = 1 \text{ GHz}$, $|\mathbf{B}| = 1 \text{ T}$, $T = 20 \text{ K}$, $\bar{\mu} = 10 \text{ meV}$, and $|\delta\mu| = 1 \text{ meV}$. The resulting aCME current density is generally of the same order of magnitude as for the case of unequal Fermi velocities, and for adiabatic pumping by a cosine input signal, the output is again shifted by a phase $-\pi$, i.e. is a negative sine with

the same frequency as the input signal. The temperature dependence of $|\mathbf{j}_{\text{CME}}|$, which is plotted in Fig. 6 for different values of b_0 , is found to be small for small b_0 but significantly enhanced for larger values of b_0 .

VI. CONCLUSIONS

The chiral magnetic effect (1) is a non dissipative transport phenomenon induced by the chiral anomaly in chirally imbalanced systems, i.e. in non equilibrium states with finite chiral chemical potential μ_5 . In the conventional realization of CME in condensed matter experiments, the chirality imbalance is generated via the chiral anomaly itself by applying external electromagnetic fields with non vanishing $\mathbf{E} \cdot \mathbf{B}$. In this paper we presented a novel chiral magnetic effect which does not rely on an external source of chirality imbalance. Instead, the source of chirality imbalance is built into the band structure of certain materials, asymmetric Weyl semimetals (aWSMs), that break parity by means of asymmetric, i.e. non-identical, dispersion relations of their left and right chiral Weyl cones. The chirality imbalance is then generated upon pumping the system with a time-dependent non chiral current, which changes the chemical potential in the left and right chiral Weyl cones at a different rate due to their different capacities.

Chiral relaxation processes work against the build-up in the chiral charge density, allowing for a quasi stationary non-equilibrium state if the pumping rate is small compared to the chiral relaxation rate, i.e. if the pumping is adiabatic. The induced chiral chemical potential is then proportional to the pumping rate times the chiral relaxation rate, times a parameter measuring the asymmetry in the capacities of the left and right chiral Weyl cones. The aCME current induced by this chiral chemical potential will flow along the applied magnetic field according to (1), even if no electric field at all is applied to the system, or if the electric field is perpendicular to the magnetic field. The expression (1) for the CME current is valid for deformed nodal points with the Berry monopole structure (22), as long as the system is continuously connected to the undeformed, rotationally invariant case [43]. The CME current may only take a different form if the nodal point is topologically distinct, i.e. described by a different topological invariant. From its derivation it is clear that the aCME should be generic for materials with asymmetric dispersion relations as long as they are chiral, i.e. as long as the chiral relaxation time is longer than the typical time scale for electric current relaxation as extracted from the Drude model, $\tau_5 \gg \tau$.

In Sec. V, we presented a detailed experimental setup to measure the new aCME in asymmetric WSM, and estimated the induced currents quantitatively (see App. D for details). For realistic input parameters for the chemical potential, temperature and the chiral relaxation rate, we found an aCME current of the same order of magnitude, and possibly even stronger, as the conventional

CME current. For our input parameters we assumed that the values inferred for the DSM ZrTe_5 [10] are typical also for aWSMs.

Apart from the AC voltage considered above, one could also drive the system by laser. In this case the laser light will induce oscillations of charge density which can have much higher frequencies than the AC source, e.g. in the terahertz frequency range. This would yield a much stronger aCME current.

Our effect is predicted to exist in materials in which the left- and right-handed Weyl quasiparticles have different dispersion relations. Recently, such Weyl semimetals with broken reflection and inversion symmetries were predicted theoretically, with SrSi_2 as an example [22]. We urge the experimental study of aCME in this and other asymmetric Weyl semimetals, as this would greatly improve the understanding of the role that chiral anomaly plays in transport phenomena.

ACKNOWLEDGMENTS

We would like to thank Karl Landsteiner, Qiang Li, Shinsei Ryu, Maria Vozmediano and Yi Yin for useful discussions. Y.K. is supported by the Grants-in-Aid for JSPS fellows (Grant No.15J01626). The work of R.M. was supported in part by the U.S. Department of Energy under Contract No. DE-FG-88ER40388, as well as by the Alexander-von-Humboldt Foundation through a Feodor Lynen postdoctoral fellowship.

Appendix A: Computation of index for aWSMs with different Fermi velocities

In this appendix, we present the detailed computation of the index for the left chiral fermions (16). To this end, we introduce a cutoff Λ which regularizes the states with large Dirac eigenvalues,

$$\begin{aligned} & \sum_n \phi_n^*(x) \gamma_5 \phi_n(x) \\ &= \lim_{\Lambda \rightarrow \infty} \left(\sum_n \phi_n^*(x) \gamma_5 e^{-(\lambda_n/\Lambda)^2} \phi_n(x) \right) \\ &= \lim_{\Lambda \rightarrow \infty} \text{tr} \left[\gamma_5 e^{-(\not{D}_L/\Lambda)^2} \sum_n \phi_n(x) \phi_n^*(x) \right] \\ &= \lim_{\Lambda \rightarrow \infty} \int \frac{d^4 k}{(2\pi)^4} \text{tr} \left[\gamma_5 e^{-ikx} e^{-(\not{D}_L/\Lambda)^2} e^{ikx} \right], \quad (\text{A1}) \end{aligned}$$

where we have changed the basis to plane waves by,

$$\sum_n \phi_n(x) \phi_n^*(y) = \mathbf{1}_{4 \times 4} \delta(x - y) = \mathbf{1}_{4 \times 4} \int \frac{d^4 k}{(2\pi)^4} e^{-ik(x-y)}. \quad (\text{A2})$$

$\mathbf{1}_{4 \times 4}$ is the identity matrix in the spinor space. Notice that \not{D}_L , defined in (11), explicitly depends on the Fermi velocity and \not{D}_L^2 is expanded as

$$\begin{aligned} \not{D}_L^2 &= -D_0 D_0 - v_L^2 D_i D_i - b_0 b_0 - v_L^2 b_i b_i \\ &+ \frac{ie}{4} (2v_L [\gamma^0, \gamma^i] F_{0i} + v_L^2 [\gamma^i, \gamma^j] F_{ij}) \\ &+ i\gamma_5 (v_L [\gamma^0, \gamma^i] (b_0 D_i - b_i D_0) + v_L^2 [\gamma^i, \gamma^j] b_i D_j). \end{aligned} \quad (\text{A3})$$

Therefore, (A1) can be calculated as

$$\begin{aligned} &\sum_n \phi_n^*(x) \gamma_5 \phi_n(x) \\ &= \lim_{\Lambda \rightarrow \infty} \int \frac{d^4 k}{(2\pi)^4} \\ &\times \text{tr} \left[\gamma_5 \exp \left(\frac{(ik_0 + D_0)^2 + v_L^2 (ik_i + D_i)^2}{\Lambda^2} + \frac{b_0^2 + v_L^2 b_i^2}{\Lambda^2} \right. \right. \\ &- \frac{ie}{4\Lambda^2} (2v_L [\gamma^0, \gamma^i] F_{0i} + v_L^2 [\gamma^i, \gamma^j] F_{ij}) \\ &- \left. \left. \frac{i}{\Lambda^2} \gamma_5 (v_L [\gamma^0, \gamma^i] (b_0 D_i - b_i D_0) + v_L^2 [\gamma^i, \gamma^j] b_i D_j) \right) \right] \\ &= \frac{1}{16\pi^2 v_L^3} \\ &\times \text{tr} \frac{1}{2} \left[\gamma_5 \left(\frac{ie}{4} (2v_L [\gamma^0, \gamma^i] F_{0i} + v_L^2 [\gamma^i, \gamma^j] F_{ij}) \right)^2 \right] \\ &= \frac{e^2}{32\pi^2} \epsilon^{\mu\nu\alpha\beta} F_{\mu\nu} F_{\alpha\beta}. \end{aligned} \quad (\text{A4})$$

In the final equality, we have used the identity

$$\text{tr}[\gamma^5 \gamma^\mu \gamma^\nu \gamma^\alpha, \gamma^\beta] = -4\epsilon^{\mu\nu\alpha\beta}, \quad (\text{A5})$$

in Euclidean signature. Note that v_L drops out due to picking up the cross term in the final equality of (A4).

Appendix B: Finite temperature expressions for aWSMs with different Fermi velocities

In this appendix, we present the finite temperature expression of the aCME current. The left Weyl node contribution to the current is given by

$$\begin{aligned} j_{\text{CME},L} &= e^2 \mathbf{B} \int_{\mathbf{p}} f_{\mathbf{p}} \left(\boldsymbol{\Omega} \cdot \frac{\partial \epsilon_{\mathbf{p}}}{\partial \mathbf{p}} \right) \\ &= \frac{e^2 \mathbf{B}}{4\pi^2} T \ln(1 + e^{(\mu_L + E_0)/T}) \\ &= \frac{e^2 \mathbf{B}}{4\pi^2} (\mu_L + E_0) (1 + O(e^{-(\mu_L + E_0)/T})), \end{aligned} \quad (\text{B1})$$

where the distribution function is $f_{\mathbf{p}} = 1/(1 + e^x)$ with $x = (\epsilon_{\mathbf{p}} - \mu_L)/T$. Notice that the nontrivial temperature dependence is exponentially suppressed is suppressed at

low temperatures due to the Fermi sea cutoff E_0 [7]. Hence the net CME current is expressed as

$$\mathbf{j}_{\text{CME}} = \frac{e^2 \mathbf{B}}{2\pi^2} \mu_5. \quad (\text{B2})$$

Therefore, the expression for CME current is unchanged up to the exponentially small corrections at low temperatures.

The left and right chiral fermion densities receive a finite temperature correction

$$\rho_{L/R} = \frac{\mu_{L/R}^3 + \pi^2 T^2 \mu_{L/R} + E_0^3}{6\pi^2 v_{L/R}^3} (1 + O(e^{-(\mu_{L/R} + E_0)/T})). \quad (\text{B3})$$

At finite temperature, Eqs. (33) and (34) become

$$\begin{aligned} v_L^3 \delta \rho_L - v_R^3 \delta \rho_R &= \frac{\tau_5}{1 + i\omega\tau_5} \frac{d\rho(t)}{dt} \frac{v_L^3 - v_R^3}{2}, \\ &= \left(\frac{\mu^2}{\pi^2} + \frac{T^2}{3} \right) \mu_5. \end{aligned} \quad (\text{B4})$$

The finite temperature version of (35) can be read off,

$$\mu_5 = \frac{\pi^2 \hbar^3 (v_L^3 - v_R^3) \tau_5}{2(\mu^2 + \pi^2 T^2/3)} \frac{\tau_5}{1 + i\omega\tau_5} \frac{d\rho(t)}{dt}. \quad (\text{B5})$$

The relation between the particle number density and chemical potential is

$$\begin{aligned} \rho(t) &= \frac{1}{6\pi^2 \hbar^3} \left(\frac{\mu_L^3 + \pi^2 T^2 \mu_L + E_0^3}{v_L^3} + \frac{\mu_R^3 + \pi^2 T^2 \mu_R + E_0^3}{v_R^3} \right) \\ &= \frac{\mu^3 + \pi^2 T^2 \mu + E_0^3}{6\pi^2 \hbar^3} \left(\frac{1}{v_L^3} + \frac{1}{v_R^3} \right) \left(1 + O\left(\frac{\Delta v}{V} \frac{\mu_5}{\mu} \right) \right), \end{aligned} \quad (\text{B6})$$

which leads to

$$\frac{d\rho(t)}{dt} = \frac{3\mu^2 + \pi^2 T^2}{6\pi^2 \hbar^3} \left(\frac{1}{v_L^3} + \frac{1}{v_R^3} \right) \frac{d\mu}{dt} \left(1 + O\left(\frac{\Delta v}{V} \frac{\mu_5}{\mu} \right) \right). \quad (\text{B7})$$

Therefore, the chiral chemical potential is

$$\mu_5 = \frac{(v_L^6 - v_R^6)}{4v_L^3 v_R^3} \frac{d\mu(t)}{dt} \tau_5 \simeq \frac{3}{2} \frac{\Delta v}{V} \frac{\tau_5}{1 + i\omega\tau_5} \frac{d\mu(t)}{dt}. \quad (\text{B8})$$

Finally, the aCME current is given by

$$\mathbf{j}_{\text{CME}} = \frac{3e^2}{4\pi^2 \hbar^2 c} \frac{\Delta v}{V} \frac{\tau_5}{1 + i\omega\tau_5} \frac{d\mu}{dt} \mathbf{B}. \quad (\text{B9})$$

By using $\mu(t) = \bar{\mu} + \delta\mu(t)$ with $\delta\mu(t) \propto e^{i\omega t}$ and taking the real part of (B9),

$$\mathbf{j}_{\text{CME}} = \frac{3e^2}{4\pi^2 \hbar^2 c} \frac{\Delta v}{V} \frac{(\omega\tau_5)^2 \cos \omega t - \omega\tau_5 \sin(\omega t)}{1 + (\omega\tau_5)^2} |\delta\mu| \mathbf{B}. \quad (\text{B10})$$

Note that to $O((\Delta v/V)(\mu_5/\mu))$, the temperature dependence completely cancelled between (B5) and (B7). This is a special feature of the chosen dispersion and approximation, which e.g. does not happen in the energy separated aWSM of App.D.

Appendix C: aCME with energy separation between Weyl nodes

The aCME is also realized in materials with finite energy separation between the left and right Weyl nodes, denoted by b_0 , as depicted in Fig.2. In this appendix, we present the aCME expression with finite b_0 instead of different right and left Fermi velocities. The particle number densities of the left and right Weyl fermions are given by

$$\rho_{L/R} = \frac{(\mu_{L/R} \mp b_0/2)^3 + \pi^2 T^2 (\mu_{L/R} \mp b_0/2) + (E_0 \pm b_0/2)^3}{6\pi^2 v_F^3}. \quad (C1)$$

Correspondingly, $\rho_{L,R}^{\text{CB}}$ and ρ_5^{CB} are given by

$$\rho_{L/R}^{\text{CB}} = \frac{(\mu_{\text{CB}} \mp b_0/2)^3 + \pi^2 T^2 (\mu_{\text{CB}} \mp b_0/2) + (E_0 \pm b_0/2)^3}{6\pi^2 v_F^3}, \quad (C2)$$

$$\rho_5^{\text{CB}} = -\frac{b_0(\mu_{\text{CB}}^2 + \pi^2 T^2/3 - E_0^2)}{2\pi^2 v_F^3}. \quad (C3)$$

Hence we obtain

$$\begin{aligned} \frac{d\delta\rho_5}{dt} &= \frac{b_0}{2\pi^2 v_F^3} \frac{d\mu_{\text{CB}}^2}{dt} - \frac{\delta\rho_5}{\tau_5} \\ &\simeq \frac{b_0\bar{\mu}}{\pi^2 v_F^3} \frac{d\delta\mu}{dt} - \frac{\delta\rho_5}{\tau_5}, \end{aligned} \quad (C4)$$

where we have used $\mu_{\text{CB}} = \mu(1 + O(\mu_5/\mu))$ and $\mu = \bar{\mu} + \delta\mu$ with $|\delta\mu| \ll \bar{\mu}$. By assuming $\delta\mu \propto e^{i\omega t}$, we obtain the solution,

$$\delta\rho_5 = \frac{b_0\bar{\mu}}{\pi^2 v_F^3} \frac{\tau_5}{1 + i\omega\tau_5} \frac{d\mu}{dt}, \quad (C5)$$

In terms of μ_5 , $\delta\rho_5$ can be expressed as

$$\delta\rho_5 = \frac{\mu^2 + \pi^2 T^2/3 + b_0^2/4}{\pi^2 v_F^3} \mu_5 \quad (C6)$$

Therefore, the chiral chemical potential becomes

$$\mu_5 = \frac{b_0\bar{\mu}}{\mu^2 + \pi^2 T^2/3 + b_0^2/4} \frac{\tau_5}{1 + i\omega\tau_5} \frac{d\mu}{dt}, \quad (C7)$$

$\mu_5 \ll \mu$ is readily satisfied for $\omega\tau_5 \ll 1$. Then, the induced CME current is expressed as

$$\begin{aligned} j_{\text{CME}} &= \frac{e^2}{2\pi^2 \hbar^2 c} \frac{b_0\bar{\mu}}{\bar{\mu}^2 + \pi^2 T^2/3 + b_0^2/4} \\ &\times \frac{(\omega\tau_5)^2 \cos\omega t - \omega\tau_5 \sin(\omega t)}{1 + (\omega\tau_5)^2} |\delta\mu| \mathbf{B} \\ &\simeq -\frac{e^2}{2\pi^2 \hbar^2 c} \frac{b_0\bar{\mu}}{\bar{\mu}^2 + \pi^2 T^2/3 + b_0^2/4} |\delta\mu| \omega\tau_5 \sin(\omega t) \mathbf{B}. \end{aligned} \quad (C8)$$

Appendix D: Parameterization for CME current

The parameters in Eqs. (B9) and (C8) are given in Gaussian (CGS) units. The parameterizations given in Sec. V are expressed in Gaussian units as follows:

$$|\delta\mu| = 1 \text{ meV} = 1.6 \times 10^{-15} \text{ erg}, \quad (D1)$$

$$\Delta = 50 \text{ meV} = 8 \times 10^{-14} \text{ erg}, \quad (D2)$$

$$B = 1 \text{ T} = 1 \times 10^4 \text{ Gs}, \quad (D3)$$

$$T = 20 \text{ K} = 1.4 \times 10^{-16} \text{ erg}. \quad (D4)$$

Furthermore $e = 4.8 \times 10^{-10} \text{ Fr}$, $\hbar = 1.1 \times 10^{-27} \text{ erg s}$, and $c = 3 \times 10^{10} \text{ cm/s}$.

The result (B9) expressed in SI units reads,

$$\begin{aligned} \frac{j_{\text{CME}}}{[\text{A/m}^2]} (3 \times 10^5) &= -\frac{3(4.8 \times 10^{-10})^2}{(6.6 \times 10^{-27})^2 (3 \times 10^{10})} \\ &\times \frac{\Delta v}{V} \frac{\frac{\omega}{[\text{GHz}]} (6.6 \times 10^{-18}) \frac{|\delta\mu|}{[\text{meV}]} (1.6 \times 10^{-15})}{\frac{\Delta}{[\text{meV}]} (1.6 \times 10^{-15})} \\ &\times \frac{\mathbf{B}}{[\text{T}]} (1 \times 10^4) \sin\left(\frac{\omega}{[\text{GHz}]} \frac{t}{[\text{ns}]}\right), \end{aligned} \quad (D5)$$

which can be simplified to

$$\begin{aligned} \frac{j_{\text{CME}}}{[\text{mA/mm}^2]} &= -(1.1 \times 10^2) \frac{\Delta v}{V} \frac{\omega}{[\text{GHz}]} \frac{|\delta\mu|}{[\text{meV}]} \left(\frac{\Delta}{[\text{meV}]}\right)^{-1} \frac{\mathbf{B}}{[\text{T}]} \\ &\times \sin\left(\frac{\omega}{[\text{GHz}]} \frac{t}{[\text{ns}]}\right). \end{aligned} \quad (D6)$$

The amplitude of the induced current is calculated to be

$$\begin{aligned} 7.0 \times 10^7 \text{ Fr}/(\text{s cm}^2) &= 2.2 \times 10^2 \text{ A/m}^2 \\ &= 2.2 \times 10^{-1} \text{ mA/mm}^2. \end{aligned} \quad (D7)$$

On the other hand, the result (C8) in SI units reads,

$$\begin{aligned} \frac{j_{\text{CME}}}{[\text{A/m}^2]} (3 \times 10^5) &= -\frac{2(4.8 \times 10^{-10})^2}{(6.6 \times 10^{-27})^2 (3 \times 10^{10})} \\ &\times \frac{1}{\frac{\bar{\mu}}{[\text{meV}]} / \frac{b_0}{[\text{meV}]} + (0.086\pi \times \frac{T}{[\text{K}]})^2 / \frac{3b_0\bar{\mu}}{[\text{meV}]^2} + \frac{b_0}{[\text{meV}]} / \frac{4\bar{\mu}}{[\text{meV}]}} \\ &\times \frac{\frac{\omega}{[\text{GHz}]} (6.6 \times 10^{-18}) \frac{|\delta\mu|}{[\text{meV}]} (1.6 \times 10^{-15})}{\frac{\Delta}{[\text{meV}]} (1.6 \times 10^{-15})} \frac{\mathbf{B}}{[\text{T}]} (1 \times 10^4) \\ &\times \sin\left(\frac{\omega}{[\text{GHz}]} \frac{t}{[\text{ns}]}\right), \end{aligned} \quad (D8)$$

which can be simplified to

$$\begin{aligned} \frac{j_{\text{CME}}}{[\text{mA}/\text{mm}^2]} &= -(7.4 \times 10) \\ &\times \left(\frac{\bar{\mu}}{b_0} + 0.024 \times \left(\frac{T}{[\text{K}]} \right)^2 \left(\frac{b_0 \bar{\mu}}{[\text{meV}^2]} \right)^{-1} + \frac{b_0}{4\bar{\mu}} \right)^{-1} \\ &\times \frac{\omega}{[\text{GHz}]} \frac{|\delta\mu|}{[\text{meV}]} \left(\frac{\Delta}{[\text{meV}]} \right)^{-1} \frac{B}{[\text{T}]} \sin \left(\frac{\omega}{[\text{GHz}]} \frac{t}{[\text{ns}]} \right). \end{aligned} \quad (\text{D9})$$

In addition to the aCME current, we consider the conventional CME current for comparison,

$$j_{\text{CME}} = \frac{e^4 v_F^3}{8\pi^2 \hbar c^2} \frac{\tau_5}{(\mu^2 + \pi^2 T^2)} (\mathbf{E} \cdot \mathbf{B}) \mathbf{B}. \quad (\text{D10})$$

In SI units, this reads

$$\begin{aligned} \frac{j_{\text{CME}}}{[\text{A}/\text{m}^2]} &(3 \times 10^5) \\ &= \frac{(4.8 \times 10^{-10})^4 (3 \times 10^{10}/300)^3}{8\pi^2 (3 \times 10^{10})^2} \frac{1}{\frac{\Delta}{[\text{meV}]} (1.6 \times 10^{-15})} \\ &\times \frac{1}{\left(\frac{\mu}{[\text{meV}]} (1.6 \times 10^{-15}) \right)^2 + \pi^2 \left(\frac{T}{[\text{K}]} (1.4 \times 10^{-16}) \right)^2} \\ &\times \frac{E}{[\text{V}/\text{m}]} (3 \times 10^4)^{-1} \left(\frac{B}{[\text{T}]} (1 \times 10^4) \right)^2 \\ &\times \sin \left(\frac{\omega}{[\text{GHz}]} \frac{t}{[\text{ns}]} \right), \end{aligned} \quad (\text{D11})$$

which is simplified to

$$\begin{aligned} \frac{j_{\text{CME}}}{[\text{mA}/\text{mm}^2]} &= (2.0 \times 10^3) \left(\frac{\Delta}{[\text{meV}]} \right)^{-1} \\ &\times \left(\left(\frac{\mu}{[\text{meV}]} \right)^2 + (7.6 \times 10^{-2}) \left(\frac{T}{[\text{K}]} \right)^2 \right)^{-1} \frac{E}{[\text{V}/\text{m}]} \left(\frac{B}{[\text{T}]} \right)^2 \\ &\times \sin \left(\frac{\omega}{[\text{GHz}]} \frac{t}{[\text{ns}]} \right). \end{aligned} \quad (\text{D12})$$

For $\Delta = 50[\text{meV}]$, $\mu = 10[\text{meV}]$, $T = 0[\text{K}]$, $E = 0.1[\text{mV}/\text{mm}]$, and $B = 1[\text{T}]$, the amplitude of the current becomes $4.0 \times 10^{-1}[\text{mA}/\text{mm}^2]$. We obtain the amplitude $4.0 \times 10[\text{mA}/\text{mm}^2]$ if we increase the magnetic field to $B = 10[\text{T}]$.

-
- [1] K. Fukushima, D. E. Kharzeev, and H. J. Warringa, Phys. Rev. **D78**, 074033 (2008), arXiv:0808.3382 [hep-ph].
- [2] D. E. Kharzeev, Prog. Part. Nucl. Phys. **75**, 133 (2014), arXiv:1312.3348 [hep-ph].
- [3] D. E. Kharzeev, K. Landsteiner, A. Schmitt, and H.-U. Yee, Lect. Notes Phys. **871**, 1 (2013), arXiv:1211.6245 [hep-ph].
- [4] D. T. Son and N. Yamamoto, Phys. Rev. Lett. **109**, 181602 (2012), arXiv:1203.2697 [cond-mat.mes-hall].
- [5] D. T. Son and B. Z. Spivak, Phys. Rev. **B88**, 104412 (2013), arXiv:1206.1627 [cond-mat.mes-hall].
- [6] A. A. Zyuzin and A. A. Burkov, Phys. Rev. **B86**, 115133 (2012), arXiv:1206.1868 [cond-mat.mes-hall].
- [7] G. Basar, D. E. Kharzeev, and H.-U. Yee, Phys. Rev. **B89**, 035142 (2014), arXiv:1305.6338 [hep-th].
- [8] M. Vazifeh and M. Franz, Physical review letters **111**, 027201 (2013).
- [9] P. Goswami and S. Tewari, Physical Review B **88**, 245107 (2013).
- [10] Q. Li, D. E. Kharzeev, C. Zhang, Y. Huang, I. Pletikoscic, A. V. Fedorov, R. D. Zhong, J. A. Schneeloch, G. D. Gu, and T. Valla, (2014), 10.1038/nphys3648, arXiv:1412.6543 [cond-mat.str-el].
- [11] H.-J. Kim, K.-S. Kim, J.-F. Wang, M. Sasaki, N. Satoh, A. Ohnishi, M. Kitaura, M. Yang, and L. Li, Physical review letters **111**, 246603 (2013).
- [12] J. Xiong, S. K. Kushwaha, T. Liang, J. W. Krizan, M. Hirschberger, W. Wang, R. Cava, and N. Ong, Science **350**, 413 (2015).
- [13] C.-Z. Li, L.-X. Wang, H. Liu, J. Wang, Z.-M. Liao, and D.-P. Yu, Nature communications **6** (2015).
- [14] X. Huang, L. Zhao, Y. Long, P. Wang, D. Chen, Z. Yang, H. Liang, M. Xue, H. Weng, Z. Fang, *et al.*, Physical Review X **5**, 031023 (2015).
- [15] Z. Wang, Y. Zheng, Z. Shen, Y. Zhou, X. Yang, Y. Li, C. Feng, and Z.-A. Xu, arXiv preprint arXiv:1506.00924 (2015).
- [16] C. Zhang, S.-Y. Xu, I. Belopolski, Z. Yuan, Z. Lin, B. Tong, N. Alidoust, C.-C. Lee, S.-M. Huang, H. Lin, *et al.*, arXiv preprint arXiv:1503.02630 (2015).
- [17] X. Yang, Y. Li, Z. Wang, Y. Zhen, and Z.-a. Xu, arXiv preprint arXiv:1506.02283 (2015).
- [18] C. Shekhar, F. Arnold, S.-C. Wu, Y. Sun, M. Schmidt,

- N. Kumar, A. G. Grushin, J. H. Bardarson, R. D. d. Reis, M. Naumann, *et al.*, arXiv preprint arXiv:1506.06577 (2015).
- [19] X. Yang, Y. Liu, Z. Wang, Y. Zheng, and Z.-a. Xu, arXiv preprint arXiv:1506.03190 (2015).
- [20] D. Kharzeev, *Annals of Physics* **325**, 205 (2010).
- [21] For the purpose of the conventional chiral anomaly induced chiral magnetic effect the two overlapping Weyl cones of a DSM contribute in the same way as for a WSM. We will see that this is not the case for the asymmetric CME discussed in this work, which vanishes in DSMs with exactly coinciding dispersion relations such as e.g. ZrTe_5 [10].
- [22] S.-M. Huang, S.-Y. Xu, I. Belopolski, C.-C. Lee, G. Chang, T.-R. Chang, B. Wang, N. Alidoust, G. Bian, M. Neupane, *et al.*, *Proceedings of the National Academy of Sciences* **113**, 1180 (2016).
- [23] S. Murakami, *New Journal of Physics* **9**, 356 (2007).
- [24] D. E. Kharzeev and H.-U. Yee, *Phys. Rev. D* **84**, 045025 (2011), arXiv:1105.6360 [hep-th].
- [25] B.-J. Yang and N. Nagaosa, *Nature communications* **5** (2014).
- [26] A. Burkov, *Journal of Physics: Condensed Matter* **27**, 113201 (2015).
- [27] H. B. Nielsen and M. Ninomiya, *Physics Letters B* **105**, 219 (1981).
- [28] H. B. Nielsen and M. Ninomiya, *Nuclear Physics B* **185**, 20 (1981).
- [29] H. B. Nielsen and M. Ninomiya, *Nuclear Physics B* **193**, 173 (1981).
- [30] E. Kiritsis, *Commun. Math. Phys.* **111**, 417 (1987).
- [31] More precisely, since parity (P) in 3+1 dimensions acts on the spatial coordinates and momenta as $x^i \mapsto -x^i$ and $k^i \mapsto -k^i$ ($i = 1, 2, 3$), respectively, the condition for parity invariance for the low energy dispersion relation is $\omega_L(k_i) = \omega_R(-k_i)$, i.e. for a left chiral Weyl node at spatial momentum \mathbf{k} , there exists an identical right chiral node at momentum $-\mathbf{k}$. Time reversal (T) on the other hand sends $\mathbf{k} \mapsto -\mathbf{k}$ but does not exchange chiralities, and hence Weyl nodes must exist in pairs of the same chirality but at opposite momenta in the Brillouin zone.
- [32] Here, Lorentz symmetry is preserved for each Weyl cone separately, but broken since the left and right handed Weyl fermions do not have the same velocities, i.e. do not travel on an overall universal light cone.
- [33] G. Hooft, *Recent Developments in Gauge Theories*, 135 (1980).
- [34] Y. Frishman, A. Schwimmer, T. Banks, and S. Yankielowicz, *Nucl. Phys. B* **177**, 157 (1981).
- [35] The dots represent additional parameters such as the different Fermi velocities for each chirality, or the different tilting parameters for type I/II Weyl semimetals. They also include necessary physical cutoffs, as well as the Dirac sea cutoff.
- [36] As shown in App. C, b_0 will however be responsible for an aCME response in the presence of an external non chiral pumping current.
- [37] K. Fujikawa and H. Suzuki, *Path integrals and quantum anomalies* (Clarendon Press, 2004).
- [38] With this definition of the 4×4 Dirac operator it is known that the following procedure yields the covariant anomaly in the system where the chiral Weyl fermions couple to the external gauge field. See [37] for detailed explanation.
- [39] M. A. Stephanov and Y. Yin, *Phys. Rev. Lett.* **109**, 162001 (2012), arXiv:1207.0747 [hep-th].
- [40] J.-W. Chen, S. Pu, Q. Wang, and X.-N. Wang, *Phys. Rev. Lett.* **110**, 262301 (2013), arXiv:1210.8312 [hep-th].
- [41] This is a necessary condition for the system to be approximately chiral, i.e. a WSM: If the chiral charge would relax faster than the electric current, the chirality of the Weyl fermions would not be approximately preserved on electric transport timescales, and transport would be effectively non-chiral.
- [42] Typical CPU frequencies in modern day computers are of this order, limited basically by the optical limit for inter band transitions in the semiconductors used, generating large thermal losses.
- [43] J.-h. Gao and Q. Wang, *Phys. Lett. B* **749**, 542 (2015), arXiv:1504.07334 [nucl-th].
- [44] K. Landsteiner (2016) arXiv:1610.04413 [hep-th].